UNIVERSITÉ CÔTE D'AZUR

Accelerated Simulation of Cardiac Arrhythmias by Projective Integration on Unstructured Meshes

SINADINOVIC Marko

Optional Thesis approved by **Prof. Thomas REY**

Acknowledgements

Abstract

Résumé FR ?

Contents

Introduction

Cardiac Arrhythmias and Re-entry Mechanisms

Cardiovascular diseases remain the leading cause of death globally accounting for nearly 18 million deaths annually. Sudden cardiac death is particularly dangerous because it often strikes without warning. The root cause is usually an arrhythmia which is a disruption in the synchronized electrical signals that coordinate the heart's contraction.

In a healthy heart an electrical wave starts at the sinoatrial node and sweeps through the tissue triggering a beat and then extinguishing itself to let the tissue recover. In pathological cases such as after a heart attack where scar tissue forms this wave can get trapped. Instead of extinguishing the wave curls around an obstacle and re-enters tissue that has already recovered.

This phenomenon creates a self-sustaining short circuit. The electrical wave begins to rotate forming a spiral wave. If this spiral breaks up into multiple chaotic waves the result is ventricular fibrillation, the heart stops pumping blood and simply quivers. Without immediate electrical defibrillation death follows in minutes. Understanding the dynamics of these spiral waves is therefore not just a mathematical curiosity, it is a critical step toward better treatments and digital twin technologies for patient specific therapy.

Multi-scale Stiffness in Cardiac Electrophysiology

Simulating these arrhythmias on a computer is difficult due to the multi-scale nature of the problem. We are trying to model a macroscopic organ in centimeters based on microscopic cell kinetics in micrometers. From a mathematical perspective the equations governing cardiac electricity are stiff. The fast scale is the initial excitation of a cell which happens incredibly fast in less than 1 millisecond and to capture this physics accurately a numerical simulation must use a tiny time step denotes as Δt. The slow scale is the recovery phase is very slow lasting up to 300 milliseconds.

To remain stable during the fast phase the solver is forced to take millions of microscopic steps even during the slow phases where nothing much is happening. This makes simulating even a few seconds of heart activity computationally expensive often taking hours or days on standard hardware. For clinical applications requiring real-time feedback this is unacceptable.

Real-time Simulation using High-Performance Computing

The primary objective is to overcome this computational bottleneck. We aim to develop a high-performance simulation engine capable of modeling cardiac arrhythmias in 2D heterogenous media significantly faster than standard methods.

Our strategy rests on three pillars designed to optimize both accuracy and computational speed. First to address the temporal stiffness we implement an Explicit Projective Integration scheme known as PFE. By exploiting the spectral gap between the fast excitation and slow recovery scales this method allows the solver to project the solution forward in time effectively bypassing redundant calculations during the slow phases of the cardiac cycle.

Complementing this temporal acceleration we ensure spatial fidelity through the Finite Element Method (FEM) on unstructured triangular meshes. This approach offers the geometric flexibility required to accurately model complex anatomical features and local tissue heterogeneities such as fibrotic regions. The solver

is developed in C++ with the Eigen library for optimized linear algebra and OpenMP for parallel execution ensuring that the simulation maximizes the throughput of modern multi-core processors.

Chapter 1

Mathematical Modeling of Excitable Media

1.1 From Cell to Tissue : Principles of Reaction-Diffusion Systems

To understand how an arrhythmia propagates in the heart we must look back at physics. Historically the modeling of electrical propagation in biological tissue is deeply rooted in the theory of heat conduction developed by Fourier in the 19th century and the cable theory later applied to nerves by Lord Kelvin

1.1.1 The Analogy with Heat Diffusion

Cardiac tissue acts like a wet cable. When a cell depolarizes i.e. becomes positive it creates a voltage difference with its resting neighbors. Current flows from high potential to low potential mimicking the flow of heat from a hot region to a cold one.

Mathematically if the heart were a passive block of material, the potential V would simply obey the classical heat equation :

$$\frac{\partial V}{\partial t} = \nabla \cdot (\mathbf{D} \nabla V) \tag{1.1}$$

Here the diffusion operator $\nabla \cdot (\mathbf{D} \nabla V)$ acts to smooth out spatial differences eventually leading to a uniform equilibrium.

1.1.2 Adding the Reaction Term

Cardiac tissue is not just a passive wire, it is an active excitable medium. Unlike a cable where signals fade over distance the heart regenerates the electrical impulse as it travels. This ensures the signal from the sinoatrial node, a part of the heart that generates an electrical signal that causes the upper heart chambers to contract, reaches the furthest cells with full strength allowing for a synchronized contraction.

To capture this, we augment the heat equation with a non-linear source term transforming it into a Reaction-Diffusion equation. This leads to the Monodomain Model our the governing equation :

1.1.3 The Monodomain Equation

The most widely used mathematical description for tissue level electrophysiology is the Monodomain Model. It describes the evolution of the transmembrane potential V_m (mV) as a balance between the local cellular currents and the intercellular coupling.

Deriving from the conservation of charge the governing Partial Differential Equation (PDE) is defined on the domain $\Omega \subset \mathbb{R}^2$ as :

$$\underbrace{\chi C_m \frac{\partial V_m}{\partial t}}_{\text{Time Evolution}} = \underbrace{\nabla \cdot (\mathbf{D} \nabla V_m)}_{\text{Diffusion (Heat)}} - \underbrace{\chi I_{\text{ion}}(V_m, \mathbf{u})}_{\text{Reaction (Source)}} \tag{1.2}$$

Where :

- χ represents the surface-to-volume ratio of the cells (cm^{-1}).
- C_m is the specific membrane capacitance ($\mu F/cm^2$).
- $\mathbf{D}$ is the diffusion tensor capturing the anisotropy of the tissue.

- $I_{\text{ion}}(V_m, \mathbf{u})$ is the total ionic current density ($\mu F/cm^2$) which depends non-linearly on the potential V_m and a set of state variables $\mathbf{u}$ concentrations.
- I_{stim} is an external stimulation current used to artificially initiate a wave.

Mathematically it's a semilinear parabolic PDE. The diffusive term $\nabla \cdot (\mathbf{D}\nabla V_m)$ tends to smooth spatial gradients while the reactive term I_{ion} tries to regenerate the wavefront and maintain its shape. It is this balance that allows the heart to propagate a signal over long distances without signal loss. A phenomenon known as a traveling wave which is fundamentally different from simple diffusion.

1.1.4 Anisotropy and the Diffusion Tensor

In the standard heat equation diffusion is often isotropic. In the heart this is not the case. The tissue is composed of muscle fibers arranged in complex laminar sheets. Electricity flows significantly faster along these fibers than across them.

A feature of cardiac tissue is its anisotropy. Electrical waves propagate faster along the muscle fibers than transverse to them. In our model this is encoded in the diffusion tensor $\mathbf{D}$.

To visualize this anisotropy let us consider a 2D local coordinate system where the muscle fibers are oriented at an angle $\theta(\mathbf{x})$ relative to the x-axis. The fiber direction vector is given by $\mathbf{f} = (\cos\theta, \sin\theta)^T$.

Substituting this into the tensor definition the diffusion tensor $\mathbf{D}$ takes the explicit matrix form :

$$\mathbf{D} = \underbrace{\begin{pmatrix} \cos\theta & -\sin\theta \\ \sin\theta & \cos\theta \end{pmatrix}}_{\text{Rotation } R_\theta} \underbrace{\begin{pmatrix} \sigma_L & 0 \\ 0 & \sigma_T \end{pmatrix}}_{\text{Eigenvalues}} \underbrace{\begin{pmatrix} \cos\theta & \sin\theta \\ -\sin\theta & \cos\theta \end{pmatrix}}_{\text{Rotation } R_\theta^T} \tag{1.3}$$

By expanding this product we obtain the symmetric conductivity matrix used in the Finite Element assembly :

$$\mathbf{D} = \begin{pmatrix} \sigma_L \cos^2\theta + \sigma_T \sin^2\theta & (\sigma_L - \sigma_T)\cos\theta\sin\theta \\ (\sigma_L - \sigma_T)\cos\theta\sin\theta & \sigma_L \sin^2\theta + \sigma_T \cos^2\theta \end{pmatrix} \tag{1.4}$$

Formally :

$$\mathbf{D}(\mathbf{x}) = \sigma_L \mathbf{f}(\mathbf{x}) \otimes \mathbf{f}(\mathbf{x}) + \sigma_T(\mathbf{I} - \mathbf{f}(\mathbf{x}) \otimes \mathbf{f}(\mathbf{x})) \tag{1.5}$$

Where $\mathbf{f}(\mathbf{x})$ is the unit vector, σ_L and σ_T are the conductivities in the longitudinal (parallel to fibers) and transverse directions respectively. When $\theta \neq 0°$ or $90°$ the off-diagonal terms are non-zero. This means that flux in the x-direction induces a voltage change in the y-direction a phenomenon known as the cross-diffusion effect.

1.1.5 Boundary Conditions

To obtain a unique solution we must specify how the electrical potential behaves at the physical boundaries of the heart denoted by $\partial\Omega$.

Physiologically the myocardium is surrounded by tissues, like lungs and fat, that have a significantly lower electrical conductivity compared to the cardiac muscle itself. We will adopt the standard assumption of an isolated heart. This implies that no electrical current can flow out of the domain into the surrounding medium.

Mathematically this corresponds to a Homogeneous Neumann Boundary Condition. Due to the anisotropy described in Equation (1.3) the no lux condition must align with the diffusion tensor not just the geometry :

$$-(\mathbf{D}\nabla V_m) \cdot \mathbf{n} = 0 \quad \text{on } \partial\Omega \tag{1.6}$$

where $\mathbf{n}$ is the unit normal vector pointing outward from the boundary surface. This condition is particularly advantageous for the FEM formulation. Being a natural boundary condition in the weak formulation it requires no explicit enforcement in the system matrix assembly because the boundary integral simply

vanishes.

Now we must look at the overall phenomenon which is the form of the action potential and create an equation that reproduces it.

1.2 The Aliev-Panfilov Model

To solve the Monodomain Equation (1.2) we must explicitly define the ionic current term I_{ion}. In computational cardiac electrophysiology two main modeling approaches exist :

1. **Biophysical Models** (e.g., Luo-Rudy, Ten Tusscher) : These models aim for microscopic realism by explicitly representing dozens of ion channels ($I_{Na}, I_{K1}, I_{CaL}, \dots$). While highly accurate they typically involve 20 to 50 coupled differential equations per mesh node. This makes them computationally prohibitive for large-scale spatial simulations on standard hardware.
2. **Phenomenological Models** (e.g., FitzHugh-Nagumo) : These simplify the system to a minimal set of variables (excitation variable u and a recovery variable v) capturing the essential macroscopic dynamics without detailing the underlying protein kinetics.

Given our objective of real-time simulation on unstructured meshes using projective integration we adopt the phenomenological approach.

1.2.1 Phenomenological Derivation: Beyond FitzHugh-Nagumo

The classic FitzHugh-Nagumo model originally derived for nerve impulses fails to reproduce what is called restitution which is a critical property of cardiac tissue. In a real heart the duration of the Action Potential shortens as the pacing rate increases. The standard FitzHugh-Nagumo model model lacks this frequency dependence which is essential for the formation and stability of spiral waves i.e. stability of re-entry.

Aliev and Panfilov proposed a modification in 1996 to address this limitation. They introduced a variable stiffness parameter $\epsilon(u, v)$ and a specific non-linear coupling that reshapes the recovery phase to fit the restitution curve of canine myocardium.

The resulting dimensionless system governing the local kinetics is given by:

$$\begin{cases} \dfrac{\partial u}{\partial t} = \underbrace{\nabla \cdot (\mathbf{D}\nabla u)}_{\text{Diffusion}} - \underbrace{ku(u-\alpha)(u-1)}_{\text{Fast Excitation}} - \underbrace{uv}_{\text{Coupling}} \\ \dfrac{\partial v}{\partial t} = \underbrace{\epsilon(u,v) \cdot (-v - ku(u-\alpha-1))}_{\text{Slow Recovery}} \end{cases} \tag{1.7}$$

1. The Fast Variable Equation (Potential u)

- **Term :** $\nabla \cdot (\mathbf{D}\nabla u)$
  - **Mathematically :** This is the Laplacian operator generalized for anisotropic media. It acts as a smoothing term reducing spatial gradients. In the absence of reaction it would lead to a uniform distribution of u also called equilibrium.
  - **Biologically :** Represents the current flow through gap junctions. These protein channels connect adjacent cells allowing ions to diffuse from a depolarized cell to its resting neighbors thereby propagating the electrical wave across the tissue syncytium which is a tissue composed by cells resulting from the fusion of several cells.
- **Term :** $ku(u-\alpha)(u-1)$
  - **Mathematically :** This cubic polynomial provides the source of non-linearity. It introduces three roots: 0 (rest), 1 (excited), and α (threshold). It creates a bistable system where the state is driven rapidly away from the unstable threshold a towards either 0 or 1. The parameter k scales the magnitude of this drive effectively determining the stiffness of the wavefront.

- **Biologically :** Mimics the fast Sodium current denoted as I_{Na}. Once the membrane potential exceeds a critical threshold, $\alpha \approx -60$mV physically, voltage gated Na^+ channels open en masse, causing a rapid influx of positive ions and a steep upstroke (depolarization) of the action potential.

- **Term :** $-uv$
  - **Mathematically :** This is a negative feedback term. As the recovery variable v increases this term becomes more negative eventually overpowering the cubic excitation term and forcing the derivative $\frac{\partial u}{\partial t}$ to become negative.
  - **Biologically :** Represents the sum of repolarizing currents primarily the outward Potassium currents (I_{K1}, I_{Kr}, I_{Ks}). These currents work to return the cell to its resting potential terminating the action potential.

2. The Slow Variable Equation (Recovery v)

- **Term :** $\epsilon(u, v)$
  - **Mathematically :** A small scaling factor ($0 < \epsilon \ll 1$). It constrains the rate of change of v ensuring that the recovery dynamics occur on a much slower time scale than the excitation.
  - **Biologically :** Reflects the slow kinetics of ion channel gating variables. This slowness is responsible for the plateau phase of the cardiac cycle.

- **Term :** $(-v - ku(u - \alpha - 1))$
  - **Mathematically :** Defines the target value i.e. nullcline towards which v relaxes. When the cell is excited ($u \approx 1$) v is driven towards a high value, when at rest ($u \approx 0$) v relaxes back to 0.
  - **Biologically :** Represents the refractoriness of the tissue. As v rises the cell becomes unexcitable (refractory period) preventing tetany (sustained contraction) which would be fatal for the heart's pumping function.

3. The Weighting Function $\epsilon(u, v)$

$$\epsilon(u, v) = \epsilon_0 + \frac{\mu_1 v}{u + \mu_2} \tag{1.8}$$

This is the specific innovation of the Aliev-Panfilov model.

- **Mathematically :** It makes the time-scale separation state-dependent. When the cell is excited (large u) the denominator increases making ϵ small and the recovery slow what leads formation of the plateau. During the recovery phase (low u, high v) ϵ increases accelerating the return to equilibrium.

- **Biologically (Restitution):** This function allows the model to capture the Action Potential Duration, length of time an action potential lasts in cardiac tissue, restitution. At high heart rates, short diastolic interval, the variable v does not have time to fully decay. The specific form of ϵ ensures that the next action potential is shorter. It's a protective mechanism observed in real mammalian hearts to preserve diastole time for blood filling.

1.2.2 Physical Interpretation of Parameters

Unlike biophysical models where parameters correspond to measurable channel conductances, the parameters in the Aliev-Panfilov model control the shape and topology of the wave. Their physiological correlates are as follows :

- α **(Excitation Threshold) :** This parameter defines the critical value below which the system returns to rest and above which it fires an action potential. Increasing a mimics reduced excitability making the tissue harder to depolarize.

- k **(Upstroke Velocity) :** This scaling factor controls the magnitude of the non-linear source term. A higher k results in a steeper wavefront, i.e. faster depolarization, directly influencing the conduction velocity.

- ϵ_0, μ_1, μ_2 **(Restitution & Stiffness):** These parameters tune the recovery dynamics. Specifically ϵ_0 sets the baseline ratio between the fast and slow time scales. The term $\frac{\mu_1 v}{u+\mu_2}$ ensures that the recovery rate adapts to the current state of the tissue. Since $\epsilon_0 \ll 1$ the recovery process is orders of magnitude slower than excitation.

1.2.3 Stiffness Characterization

The mathematical stiffness of the system can be quantified by the ratio of time scales. The fast time scale is dominated by the upstroke $t_{\text{fast}} \approx 1/k$ while the slow recovery scale is determined by $t_{\text{slow}} \approx 1/\epsilon_0$.

For standard canine cardiac parameters, e.g. $k = 8$ and $\epsilon_0 = 0.002$, the stiffness ratio S is :

$$S \approx \frac{\tau_{\text{slow}}}{\tau_{\text{fast}}} \approx \frac{k}{\epsilon_0} = \frac{8}{0.002} = 4000 \tag{1.9}$$

This ratio implies that the fast dynamics are 4000 times faster than the slow dynamics.

1.2.4 Numerical Sensitivity Analysis

To validate the roles of these parameters, we performed a 0D sensitivity analysis using a standard adaptive ODE integrator `Isoda`. The results confirm the theoretical predictions.

Parameter Selection for Numerical Experiments

Parameter	Symbol	Value	Physical Role
Excitation Threshold	a	0.15	Controls excitability (Ischemia level)
Upstroke Scaling	k	8.0	Controls wavefront steepness ($V_{\max}$)
Base Stiffness	ϵ_0	0.002	Sets the timescale separation ratio
Restitution Scaling	μ_1	0.2	Modulates APD shortening at high rates
Restitution Shift	μ_2	0.3	Adjusts the refractory period duration

Table 1.1: **Standard Aliev-Panfilov Parameters (Canine Myocardium)**

These values correspond to the standard coefficients derived by Aliev and Panfilov to fit the electrophysiological properties of Canine Ventricular Tissue [5].

Excitability Threshold (a)

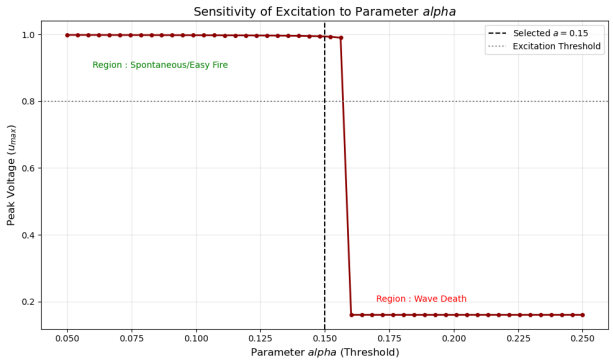

Figure 1.1: **Sensitivity of Excitation to Parameter** α

As shown in Figure 1.1 the parameter α acts as a binary switch. We stimulated the system with an initial potential $u_0 = 0.16$. For $a < 0.16$ the system excites normally ($u_{\max} \approx 1.0$). As soon as α exceeds the stimulus value the response collapses, it's wave death. This confirms that α effectively models the 1 or 0 law of cardiac tissue.

Depolarization Velocity (k)

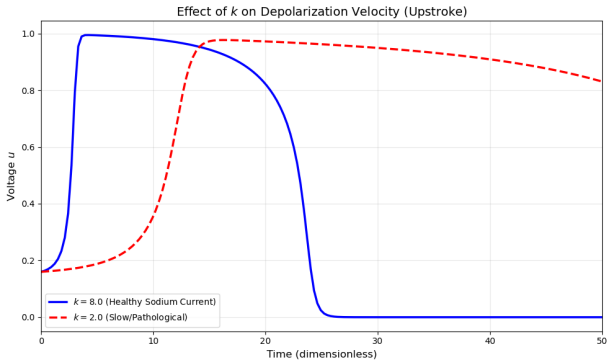

Figure 1.2: **Effect of k on Upstroke Velocity**

The influence of k on the upstroke is illustrated in Figure 1.2. A healthy value ($k = 8.0$) produces a quasi-vertical upstroke characteristic of fast Sodium channels. Reducing k to 2.0 creates a sluggish depolarization which in a spatial 2D model would result in slow conduction velocity and a higher risk of re-entry.

The Stiffness Dilemma (ϵ_0)

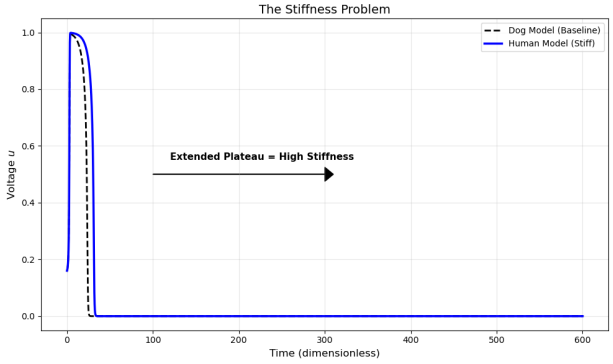

Figure 1.3: **Visualization of Stiffness**

Figure 1.3 demonstrates the root cause of the computational cost. Lowering ϵ_0 to match human physiology drastically extends the plateau phase. While the active excitation remains brief the solver is forced to integrate over a much longer duration where nothing happens (slow manifold). This visualizes the stiffness ratio S show the gap between the vertical blue line (fast) and the long horizontal tail (slow).

1.2.5 Dimensional Scaling from Canine to Human Physiology

Since the Aliev-Panfilov model is dimensionless, the variables must be scaled to match physiological units for clinical relevance. For human ventricular tissue the mapping is typically :

- **Voltage :** $V_{\text{mV}} = 100u - 80$. This linear map translates the resting state $u = 0$ to a realistic -80 mV and the peak plateau $u = 1$ to $+20$ mV.
- **Time :** The model time units (t.u.) are related to physical time by comparing the period of spiral wave rotation in the simulation to re-entrant tachycardia in biological experiments. A common conversion factor is 1 t.u. ≈ 12.9 ms.

1.3 Zero-Dimensional Analysis : Local Dynamics

Before attempting to solve the Partial Differential Equation in space it is imperative to understand the local kinetics of the single cell. This corresponds to the 0D reduction of the system where the diffusion term is set to zero.

The evolution of the system is thus governed by the following system of ODEs :

$$\begin{cases} \frac{du}{dt} = f(u,v) = ku(1-u)(u-a) - uv \\ \frac{dv}{dt} = g(u,v) = \epsilon(u,v)\left(-v - ku(u-a-1)\right) \end{cases} \tag{1.10}$$

To understand the topology of the solutions we employ phase plane analysis.

1.3.1 Phase Plane Analysis and Nullclines

The skeleton of the system's dynamics is determined by its nullclines. These are the geometric curves in the (u, v) phase plane where the temporal derivative of one variable vanishes.

The u-Nullcline (Excitation Balance)

The u-nullcline is the set of points where $\dot{u} = 0$. Solving $f(u,v) = 0$ yields :

$$\begin{aligned} & ku(1-u)(u-a) - uv = 0 \\ \iff \quad & u[k(1-u)(u-a) - v] = 0 \end{aligned} \tag{1.11}$$

This equation splits into two branches :

1. The vertical line $u = 0$ which is the resting potential.
2. The parabola $v = k(1-u)(u-a)$. This inverted parabola intersects the u-axis at $u = a$ and $u = 1$ with a maximum amplitude controlling the excitability threshold.

The v-Nullcline (Recovery Balance)

The v-nullcline is the set of points where $\dot{v} = 0$. Solving $g(u,v) = 0$ yields :

$$\begin{aligned} & -v - ku(u-a-1) = 0 \\ \iff \quad & v = -ku(u-a-1) \end{aligned} \tag{1.12}$$

This describes a second parabola opening upwards.

The intersection of these nullclines defines the fixed points of the system. Visual inspection of the graphs confirms that for standard cardiac parameters ($a \approx 0.15$) the principal intersection occurs at the origin $(0, 0)$.

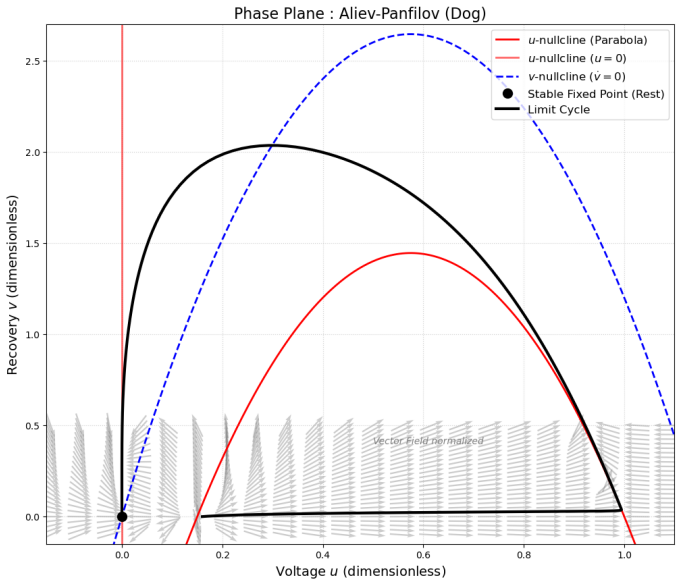

Figure 1.4: Global Phase Portrait of the Aliev-Panfilov System for canine heart

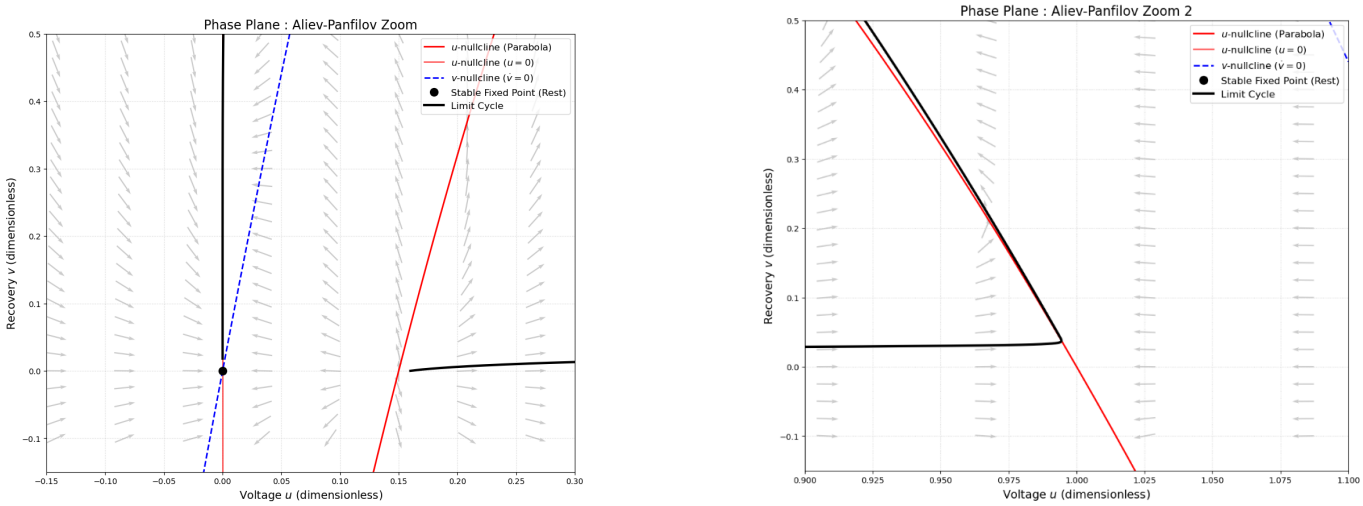

(a) Stability at the Origin

(b) Dynamics of the Plateau Phase

Figure 1.5: Local Analysis of Critical Manifolds

1.3.2 Linear Stability Analysis

To determine whether the heart tissue remains at rest or spontaneously excites we must analyze the stability of the fixed point $\mathbf{x}^* = (0, 0)$.

> **Theorem Hartman-Grobman :** Near a hyperbolic fixed point $\mathbf{x}^*$ the phase portrait of a non-linear dynamical system $\frac{dx}{dt} = \mathbf{F}(\mathbf{x})$ is topologically equivalent to its linearization $\frac{dx}{dt} = \mathbf{J}(\mathbf{x}^*)\mathbf{x}$ where $\mathbf{J}$ is the Jacobian matrix of partial derivatives.

This theorem allows us to predict the local non-linear behavior by simply computing the eigenvalues of the Jacobian matrix. Remember the Jacobian $\mathbf{J}$ is defined as :

$$\mathbf{J}(u, v) = \begin{pmatrix} \frac{\partial f}{\partial u} & \frac{\partial f}{\partial v} \\ \frac{\partial g}{\partial u} & \frac{\partial g}{\partial v} \end{pmatrix} \tag{1.13}$$

Let us compute the partial derivatives at the origin $(0, 0)$. Note that at rest $\epsilon(0, 0) = \epsilon_0 + \frac{\mu_1 \cdot 0}{0+\mu_2} = \epsilon_0$. By calculating each derivative, which is straightforward, we obtain the following linearized system matrix at the resting state :

$$\mathbf{J}(0, 0) = \begin{pmatrix} -ka & 0 \\ \epsilon_0 k(a + 1) & -\epsilon_0 \end{pmatrix} \tag{1.14}$$

Since the matrix is lower triangular the eigenvalues λ are simply the diagonal entries :

$$\lambda_1 = -ka \qquad \lambda_2 = -\epsilon_0 \quad \text{and} \quad \sigma(J) = \{\lambda_1, \lambda_2\} \tag{1.15}$$

Given that the model parameters $k > 0$, $a > 0$ and $\epsilon_0 > 0$. The eigenvalues are real and strictly negative:

$$\lambda_1 < 0, \quad \lambda_2 < 0$$

The fixed point $(0, 0)$ is a stable node called sink. Physiologically this proves that the generic state of the cardiac cell is the resting potential. The system will not generate an action potential unless it is perturbed beyond a specific threshold by an external stimulus I_{stim}.

1.3.3 The Excitation Loop

While linear analysis confirms the stability of the rest state it is the global non-linear structure of the null-clines that allows for the Action Potential.

When a stimulus pushes the state (u, v) across the middle branch of the u-nullcline, which is the threshold, the sign of $\frac{du}{dt}$ flips from negative to positive. The system is then attracted towards the excited state $(u \approx 1)$. As u increases, the slow variable v begins to rise governed by $\epsilon \ll 1$. This increase in v eventually pushes the trajectory across the u-nullcline again making $\frac{du}{dt}$ negative. The system then enters the refractory

period following the slow branch of the nullcline back to the stable equilibrium $(0, 0)$.

This excursion in the phase plane from rest, to excitation, to refractory, and back to rest corresponds exactly to the temporal profile of a heartbeat.

1.4 One-Dimensional Analysis : Wave Propagation

Having established the local kinetics we now introduce space. Physiologically this corresponds to a cable of cells such as a thin strip of ventricular muscle. To isolate the mechanism of the wavefront propagation we make a standard simplification by assuming the slow recovery variable v is frozen at zero ($v \approx 0$). This is justified by the stiffness of the system ($\epsilon \ll 1$) meaning the wave passes before the recovery variable has time to change significantly.

Under this assumption the governing Partial Differential Equation (PDE) becomes a scalar reaction-diffusion equation with a cubic non-linearity:

$$\frac{\partial u}{\partial t} = \underbrace{D\frac{\partial^2 u}{\partial x^2}}_{\text{Diffusion}} + \underbrace{ku(1-u)(u-\alpha)}_{\text{Excitation Source}} \tag{1.16}$$

1.4.1 Traveling Wave Ansatz and Coordinate Transformation

To find a solution describing a wave moving at a constant speed c we employ the Traveling Wave Ansatz. We look for a solution that maintains its shape while translating through space. Mathematically this implies that $u(x, t)$ depends only on a single moving coordinate ξ :

$$\xi = x - ct \tag{1.17}$$

Thus we define the profile function $U(\xi)$ such that $u(x, t) = U(\xi)$. By doing this we want to reduce the PDE to an ODE.

Application of the Chain Rule

First step we calculate the time derivative :

$$\frac{\partial u}{\partial t} = \frac{dU}{d\xi} \cdot \frac{\partial \xi}{\partial t} = U'(\xi) \cdot (-c) = -cU' \tag{1.18}$$

Then we calculate the space derivatives :

$$\frac{\partial u}{\partial x} = \frac{dU}{d\xi} \cdot \frac{\partial \xi}{\partial x} = U'(\xi) \cdot (1) = U' \tag{1.19}$$

Consequently the second space derivative is :

$$\frac{\partial^2 u}{\partial x^2} = \frac{d}{dx}(U') = \frac{d(U')}{d\xi} \cdot \frac{\partial \xi}{\partial x} = U''(\xi) \tag{1.20}$$

Substituting these terms back into Equation (1.16) we obtain a second-order ODE :

$$-cU' = DU'' + kU(1-U)(U-\alpha) \tag{1.21}$$

Rearranging to standard form :

$$DU'' + cU' + kU(1-U)(U-\alpha) = 0 \tag{1.22}$$

The Boundary Value Problem

This equation represents a damped mechanical system (mass D, friction c, non-linear spring force $f(U)$). For this solution to represent a valid wavefront connecting the resting tissue to the excited tissue it must satisfy these conditions :

$$\lim_{\xi \to -\infty} U(\xi) = 1 \quad \text{(Excited state behind the wave)} \tag{1.23}$$

$$\lim_{\xi \to +\infty} U(\xi) = 0 \quad \text{(Resting state ahead of the wave)} \tag{1.24}$$

1.4.2 Analytical Derivation of Conduction Velocity

Usually finding the exact wave speed c requires numerical methods. For the specific cubic non-linearity of the Aliev-Panfilov model an exact analytical solution exists.

We assume a solution trajectory in the phase plane of the form :

$$U' = -\beta U(1-U) \tag{1.25}$$

where β is a incline parameter to be determined. This implies that the spatial gradient is proportional to the potential itself.

Differentiation of (1.25) with respect to ξ yields :

$$U'' = \frac{d}{d\xi}[-\beta U(1-U)] = -\beta(1-2U)U' \tag{1.26}$$

Substituting U' from (1.25) again :

$$U'' = -\beta(1-2U)[-\beta U(1-U)] = \beta^2 U(1-U)(1-2U) \tag{1.27}$$

We inject these expressions for U' and U'' into the wave equation (1.22). Factoring out the common term $U(1-U)$ which is non-zero within the wavefront. We are left with a polynomial identity in U :

$$D\beta^2(1-2U) - c\beta + k(U-\alpha) = 0 \tag{1.28}$$

Grouping terms by powers of U :

$$\underbrace{(-2D\beta^2 + k)}_{\text{Coef. of } U} \cdot U + \underbrace{(D\beta^2 - c\beta - k\alpha)}_{\text{Constant term}} = 0 \tag{1.29}$$

For this equality to hold for all U both coefficients must vanish independently.

We solve for β :

$$-2D\beta^2 + k = 0 \implies \beta = \sqrt{\frac{k}{2D}} \tag{1.30}$$

We solve for c :

$$D\beta^2 - c\beta - k\alpha = 0 \implies c = \frac{D\beta^2 - k\alpha}{\beta} \tag{1.31}$$

Substituting $\beta^2 = k/2D$ and $\beta = \sqrt{k/2D}$:

$$c = \frac{D(\frac{k}{2D}) - k\alpha}{\sqrt{\frac{k}{2D}}} = \frac{\frac{k}{2} - k\alpha}{\sqrt{\frac{k}{2D}}} = \frac{k(\frac{1}{2} - \alpha)}{\sqrt{k}/\sqrt{2D}} \tag{1.32}$$

After simplification we obtain the fundamental formula for conduction velocity :

$$c = \sqrt{2Dk}\left(\frac{1}{2} - \alpha\right) \tag{1.33}$$

1.4.3 Analytical Sensitivity and Propagation Failure

Equation (1.33) shows the scaling laws governing the wavefront dynamics. We observe that the conduction velocity c depends non-linearly on the biophysical parameters, obeying a square-root law for diffusion and reaction rates while exhibiting a linear dependence on the excitability threshold.

The Square-Root Scaling Law (D and k)

The velocity scales as $c \propto \sqrt{Dk}$. Physically this implies that the wave speed is determined by the geometric mean of the diffusive capacity, remember D and gap junction coupling, and the reactive power k the sodium channel density. The sensitivity of the velocity to changes in diffusion is given by the partial derivative :

$$\frac{\partial c}{\partial D} = \frac{k}{2\sqrt{2Dk}} \left(\frac{1}{2} - \alpha \right) > 0 \tag{1.34}$$

This confirms that while fibrosis, equivalent a reduction in D, inevitably slows conduction, the decrease follows a $\sqrt{D}$ profile meaning that substantial structural remodeling is required to produce a significant drop in conduction velocity compared to linear decay.

The Threshold Bifurcation (α)

The linear factor $\left(\frac{1}{2} - \alpha\right)$ is the most critical term which dictates the direction of propagation.

- **Stable Propagation ($0 < \alpha < 0.5$) :** In healthy tissue $\alpha \approx 0.15$, yielding $c > 0$. The wave propagates forward invading the resting state.
- **The Standing Wave Limit ($\alpha = 0.5$) :** As the tissue becomes less excitable α increases. At the critical value $\alpha_c = 0.5$ the velocity vanishes ($c = 0$). The diffusion force exactly balances the reaction force creating a stationary wavefront.
- **Propagation Failure ($\alpha > 0.5$) :** If the threshold exceeds 0.5 the velocity becomes negative ($c < 0$). Physically the reaction term is too weak to sustain the pulse against diffusive dissipation and the wavefront collapses.

Analytically we predict the safety factor of propagation. Arrhythmias often arise in the transition zone where $\alpha \to 0.5$ creating regions of slow conduction susceptible to unidirectional block and re-entry.

1.5 Numerical Verification : 1D Finite Difference Model

Before proceeding to the complex 2D Finite Element implementation on unstructured meshes it is essential to validate our theoretical derivation of the conduction velocity. To do so we implement a lightweight 1D simulator using FMD. We discretize the continuous domain into a finite grid and approximate the derivatives.

1.5.1 Space Discretization

We define a spatial grid $x_i = i\Delta x$ for $i = 0, \ldots, N_x - 1$, where Δx is the space step. To approximate the Laplacian $\frac{\partial^2 u}{\partial x^2}$ at i we consider the Taylor expansions of u at the neighboring points $i+1$ and $i-1$:

$$u_{i+1} = u_i + \Delta x \left(\frac{\partial u}{\partial x} \right)_i + \frac{\Delta x^2}{2} \left(\frac{\partial^2 u}{\partial x^2} \right)_i + \frac{\Delta x^3}{6} \left(\frac{\partial^3 u}{\partial x^3} \right)_i + O(\Delta x^4) \tag{1.35}$$

$$u_{i-1} = u_i - \Delta x \left(\frac{\partial u}{\partial x} \right)_i + \frac{\Delta x^2}{2} \left(\frac{\partial^2 u}{\partial x^2} \right)_i - \frac{\Delta x^3}{6} \left(\frac{\partial^3 u}{\partial x^3} \right)_i + O(\Delta x^4) \tag{1.36}$$

Summing these two equations cancels the odd derivative terms (1st and 3rd order). We can then isolate the second derivative :

$$u_{i+1} + u_{i-1} = 2u_i + \Delta x^2 \left(\frac{\partial^2 u}{\partial x^2} \right)_i + O(\Delta x^4) \tag{1.37}$$

Dividing by Δx^2 we obtain the standard central difference approximation which is second-order accurate in space ($O(\Delta x^2)$) :

$$\left(\frac{\partial^2 u}{\partial x^2} \right)_i \approx \frac{u_{i+1} - 2u_i + u_{i-1}}{\Delta x^2} \tag{1.38}$$

1.5.2 Time Integration

We discretize time as $t_n = n\Delta t$. Using a first-order forward Taylor expansion for the time derivative :

$$u(x, t + \Delta t) = u(x, t) + \Delta t \frac{\partial u}{\partial t}(x, t) + O(\Delta t^2) \tag{1.39}$$

Neglecting the higher-order terms ($O(\Delta t^2)$) we approximate the derivative as :

$$\frac{\partial u}{\partial t} \approx \frac{u_i^{n+1} - u_i^n}{\Delta t} \tag{1.40}$$

Substituting this approximation and the central difference for the Laplacian into the PDE we obtain the fully discrete explicit scheme :

$$\frac{u_i^{n+1} - u_i^n}{\Delta t} = D \left[\frac{u_{i+1}^n - 2u_i^n + u_{i-1}^n}{\Delta x^2} \right] + f(u_i^n) \tag{1.41}$$

To implement this we must isolate the future state u_i^{n+1} on the left-hand side. By multiplying by Δt and rearranging terms :

$$u_i^{n+1} = u_i^n + \underbrace{\frac{D\Delta t}{\Delta x^2} \left(u_{i+1}^n - 2u_i^n + u_{i-1}^n \right)}_{\text{Diffusion Contribution}} + \underbrace{\Delta t \cdot k u_i^n (1 - u_i^n)(u_i^n - \alpha)}_{\text{Reaction Contribution}} \tag{1.42}$$

1.5.3 Stability Condition (CFL)

For this explicit scheme to remain stable, in other words errors do not grow exponentially, the CFL condition requires that :

$$\frac{D\Delta t}{\Delta x^2} \leq \frac{1}{2} \tag{1.43}$$

This imposes a strict limitation on the time step Δt relative to the spatial resolution Δx^2.

Rearranging to solve for the future state u_i^{n+1} :

$$u_i^{n+1} = u_i^n + \Delta t \left(\frac{D}{\Delta x^2} (u_{i+1}^n - 2u_i^n + u_{i-1}^n) + k u_i^n (1 - u_i^n)(u_i^n - \alpha) \right) \tag{1.44}$$

1.5.4 Boundary Conditions

The domain is isolated for this reason $\frac{\partial u}{\partial x} = 0$) which is Neumann boundary conditions. At the boundaries $i = 0$ and $i = N_x - 1$ the central difference formula (1.38) requires accessing points outside the domain u_{-1} and u_{N_x} called fictional ghost points.

Using the central difference for the first derivative :

$$\left(\frac{\partial u}{\partial x} \right)_0 \approx \frac{u_1 - u_{-1}}{2\Delta x} = 0 \implies u_{-1} = u_1 \tag{1.45}$$

Substituting $u_{-1} = u_1$ into the Laplacian formula at $i = 0$:

$$\Delta u_0 \approx \frac{u_1 - 2u_0 + u_{-1}}{\Delta x^2} = \frac{2u_1 - 2u_0}{\Delta x^2} \tag{1.46}$$

Similarly for the right boundary ($i = N_x - 1$):

$$\Delta u_{N_x - 1} \approx \frac{2u_{N_x - 2} - 2u_{N_x - 1}}{\Delta x^2} \tag{1.47}$$

These specific updates ensure mass conservation within the fiber.

1.5.5 Visualisation

To verify the analytical law we implemented the Finite Difference scheme described above. While the analytical derivation predicts propagation failure strictly at $\alpha = 0.5$ numerical simulations reveal a more complex behavior dependent on the initial conditions.

To understand this we must analyze the physical competition occurring at $t = 0$:

- **The Diffusion Term ($D\Delta u$) :** It tends to smooth out spatial gradients effectively lowering the peak of the initial stimulus. Its goal is to return the system to the equilibrium $u = 0$.
- **The Reaction Term ($f(u)$):** It drives u towards 1 but it only becomes active and self-sustaining if the local potential u remains above the threshold α for a sufficient duration.

For a wave to be successfully generated the reaction term must overcome the diffusion term before the initial energy is dissipated. This phenomenon is governed by the concept of the critical nucleus.

The Critical Nucleus Theory

There exists a critical size R_c which is the Critical Radius that the excited region must exceed to trigger a self-sustaining wave. As the medium becomes less excitable, i.e. as $\alpha \to 0.5$, the reaction force weakens and the required critical nucleus grows. Mathematically near the failure point the critical radius diverges according to the scaling :

$$R_c \propto \frac{1}{0.5 - \alpha} \tag{1.48}$$

This implies that as $\alpha \to 0.5$ the size of the tissue that must be simultaneously excited to start a wave tends towards infinity.

Sensitivity to Initial Stimulation

To demonstrate this law, we performed three sets of simulations by varying the width of the initial stimulus L_{stim} applied to the left boundary.

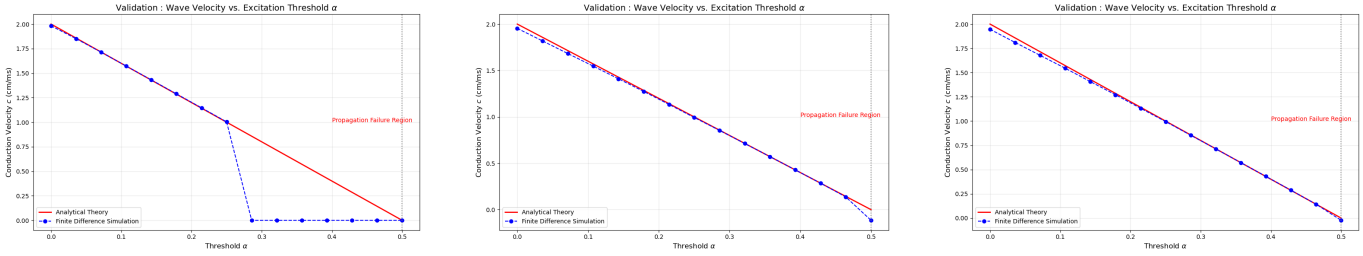

(a) $L_{\text{stim}} = 10$ (b) $L_{\text{stim}} = 25$ (c) $L_{\text{stim}} = 35$

Figure 1.6: Effect of Stimulus Energy on Wave Initiation

1. **Weak Stimulation ($L_{\text{stim}} = 10$ nodes) :** The wave dies prematurely at $\alpha \approx 0.27$ anddiffusion dissipates the energy before ignition occurs because $L_{\text{stim}} < R_c(\alpha)$
2. **Medium Stimulation ($L_{\text{stim}} = 25$ nodes) :** The wave survives longer and failling at $\alpha \approx 0.46$.
3. **Strong Stimulation ($L_{\text{stim}} = 35$ nodes) :** With this high energy input the simulation matches the theoretical prediction almost perfectly sustaining propagation up to $\alpha \approx 0.49$, nearly $L_{\text{stim}} > R_c$

These experiments validate Equation (1.33) and highlight a crucial physiological realit. In fibrotic tissue, i.e. high α, a standard electrical stimulus might fail to induce a heartbeat not because the tissue cannot carry the wave but because the stimulus is too weak to create the necessary critical nucleus.

Chapter 2

Spatial Discretization : The Finite Element Method

2.1 Weak Formulation of the Reaction-Diffusion Problem

2.1.1 Derivation using Weighted Residuals

2.1.2 Application of Green's First Identity

2.2 Galerkin Discretization on Unstructured Meshes

Delaunay Triangulation

2.2.1 Linear Lagrange Basis Functions

2.2.2 Assembly of Mass (M) and Stiffness (K) Matrices

2.3 Numerical Techniques

Mass Lumping : Diagonalization for Explicit Time-Stepping

2.3.1 Spectral Analysis : Eigenmodes of the Laplacian on Square Domains

2.3.2 Verification of the Discrete Laplacian Operator

Chapter 3

Temporal Integration: Addressing Stiffness - The Projective Method

Chapter 4

High-Performance Implementation

4.1 Software Architecture

Chapter 5

Numerical Experiments and Results

Bibliography

[1] J. Sundnes, G. T. Lines, X. Cai, B. F. Nielsen, K.-A. Mardal, and A. Tveito,
Computing the Electrical Activity in the Heart.
Springer Science & Business Media, Vol. 1, 2006.

[2] J. Keener and J. Sneyd,
Mathematical Physiology I: Cellular Physiology (2nd Edition).
Springer New York, Interdisciplinary Applied Mathematics, 2009.

[3] S. H. Strogatz,
Nonlinear Dynamics and Chaos: With Applications to Physics, Biology, Chemistry, and Engineering.
Westview Press, 2014.

[4] A. Quarteroni and A. Valli,
Numerical Approximation of Partial Differential Equations.
Springer Science & Business Media, 2008.

[5] R. R. Aliev and A. V. Panfilov,
"A simple two-variable model of cardiac excitation",
Chaos, Solitons & Fractals, vol. 7, no. 3, pp. 293–301, 1996.

[6] R. FitzHugh,
"Impulses and physiological states in theoretical models of nerve membrane",
Biophysical Journal, vol. 1, no. 6, pp. 445–466, 1961.

[7] K. H. W. J. ten Tusscher, D. Noble, P. J. Noble, and A. V. Panfilov,
"A model for human ventricular tissue",
American Journal of Physiology-Heart and Circulatory Physiology, 2004.

[8] C. W. Gear and I. G. Kevrekidis,
"Projective methods for stiff differential equations: problems with gaps in their eigenvalue spectrum",
SIAM Journal on Scientific Computing, vol. 24, no. 4, pp. 1091–1106, 2003.

[9] W. Melis,
Projective Integration for Hyperbolic Conservation Laws and Multiscale Kinetic Equations.
PhD Thesis, KU Leuven – Faculty of Engineering Science, 2017.

[10] P. Lafitte, W. Melis, and T. Rey,
"Projective integration methods for classical and quantum constraints in kinetic equations",
Kinetic & Related Models, 2016.

[11] T. Rey,
Cours sur les Équations Différentielles, EDP et Différences Finies.
Université Nice Côte d'Azur, Département de mathématiques, M1 IM, 2024.

[12] F. Berthelin,
Équations Différentielles.
Cassini, Enseignement des mathématiques, 2017.

[13] J.-P. Demailly,
Analyse Numérique et Équations Différentielles ($4^{\text{ème}}$ éd.).
EDP Sciences, 2016.